Profile of L-type Ca^{2+} current and Na^+/Ca^{2+} exchange current during cardiac action potential in ventricular myocytes

Tamas Banyasz, MD, PhD,*§ Balazs Horvath, MD, PhD,* Zhong Jian, PhD,* Leighton T. Izu, PhD,* Ye Chen-Izu, PhD*†‡

*From the *Departments of Pharmacology, †Biomedical Engineering, and ‡Internal Medicine, University of California, Davis, California; §Department of Physiology, University of Debrecen, Hungary.*

OBJECTIVE The L-type Ca^{2+} current ($I_{Ca,L}$) and the Na^+/Ca^{2+} exchange current (I_{NCX}) are major inward currents that shape the cardiac action potential (AP). Previously, the profile of these currents during the AP was determined from voltage-clamp experiments that used Ca^{2+} buffer. In this study, we aimed to obtain direct experimental measurement of these currents during cardiac AP with Ca^{2+} cycling.

METHOD A newly developed AP-clamp sequential dissection method was used to record ionic currents in guinea pig ventricular myocytes under a triad of conditions: using the cell's own AP as the voltage command, using internal and external solutions that mimic the cell's ionic composition, and, importantly, not using any exogenous Ca^{2+} buffer.

RESULTS The nifedipine-sensitive current (I_{NIFE}), which is composed of $I_{Ca,L}$ and I_{NCX}, revealed hitherto unreported features during the AP with Ca^{2+} cycling in the cell. We identified 2 peaks in the current profile followed by a long residual current extending beyond the AP, coinciding with a residual depolarization. The second peak and the residual current become apparent only when Ca^{2+} is not buffered. Pharmacological dissection of I_{NIFE} by using SEA0400 shows that $I_{Ca,L}$ is dominant during phases 1 and 2 whereas I_{NCX} contributes significantly to the inward current during phases 3 and 4 of the AP.

CONCLUSION These data provide the first direct experimental visualization of $I_{Ca,L}$ and I_{NCX} during cardiac the AP and Ca^{2+} cycle. The residual current reported here can serve as a potential substrate for afterdepolarizations when increased under pathologic conditions.

KEYWORDS Cardiac Ventricular; Myocyte; Action potential; L-type Ca^{2+} channel; Na^+/Ca^{2+} exchanger; Arrhythmia

ABBREVIATIONS **AP** = Action potential; **CDI** = Ca^{2+}-dependent inactivation; $\mathbf{I_{Ca,L}}$ = L-type Ca^{2+} current; $\mathbf{I_{NCX}}$ = Na^+/Ca^{2+} exchange current; $\mathbf{I_{NIFE}}$ = nifedipine-sensitive current; $\mathbf{I_{SEA}}$ = SEA-sensitive current

(Heart Rhythm 2012;9:134–142)

Introduction

The L-type Ca^{2+} current ($I_{Ca,L}$) and the Na^+/Ca^{2+} exchange current (I_{NCX}) are 2 major inward currents that provide the depolarization drive to shape the action potential (AP) plateau and the repolarization phase in cardiac myocytes. Changes in the magnitude or timing of these currents could cause development of cardiac arrhythmias. Hence, understanding the dynamic properties of these currents during the AP cycle is of great interest. However, the current knowledge on $I_{Ca,L}$ and I_{NCX} during the AP has been largely based on model simulations derived from traditional voltage-clamp data. Previous voltage-clamp experiments often used simplified ionic solutions to isolate the currents and used exogenous Ca^{2+} buffer—conditions that differ from the physiological milieu. In this study, we directly measured the ionic currents during the AP under a triad of conditions mimicking the physiological environment: (1) the cell's own AP was recorded and used as command voltage to directly record the $I_{Ca,L}$ and I_{NCX} during the AP; (2) the physiological ionic compositions were used in both the internal and the external solutions; and (3) the intracellular Ca^{2+} cycling during the AP was preserved by not using exogenous Ca^{2+} buffer in the internal solution.

We recorded the nifedipine-sensitive current (I_{NIFE}), which is the composite current of $I_{Ca,L}$ and I_{NCX}, during the AP with Ca^{2+} cycling. Then, we used a newly developed AP-clamp sequential dissection technique ("onion peeling")[1] to separate $I_{Ca,L}$ and I_{NCX} by using nifedipine and SEA0400. This novel experimental approach allows us, for the first time, to directly visualize the dynamics of $I_{Ca,L}$ and I_{NCX} during the AP with Ca^{2+} cycling in the cell. Our data reveal novel and distinctive features of $I_{Ca,L}$ and I_{NCX} that occur when the cell is most vulnerable to early or delayed afterdepolarizations. Measurement of the currents during the

This work was supported by NIH R grant (HL90880) to LTI, YC, and TB, NIH R03 grant (AG031944) to YC, American Heart Association National Center Scientist Development Award (0335250N) to YC, European Society of Cardiology Visiting Scientist Award to BH, and funds from the University of California to LTI and YC. **Address for reprints and correspondence:** Dr. Ye Chen-Izu, PhD, Department of Pharmacology, University of California, Davis, 2221Tupper Hall, 451 Health Science Drive, Davis, CA 95616. E-mail address: ychenizu@ucdavis.edu.

1547-5271/$ -see front matter doi:10.1016/j.hrthm.2011.08.029

AP with Ca^{2+} cycling under physiological conditions also provides realistic data to aid computational modeling and rational design of effective drug therapies for treating cardiac arrhythmias.

Methods

All laboratory procedures conform to the *Guide for the Care and Use of Laboratory Animals* published by the US National Institutes of Health.

Cell isolation

Hartley guinea pigs (male, 3–4 months old, purchased from Charles River Laboratories, USA) were first injected with heparin (800 u, intraperitoneally) and then anesthetized with nembutal (100 mg/kg, intraperitoneally). After achieving deep anesthesia to suppress spinal cord reflexes, a standard enzymatic technique was used to isolate ventricular myocytes.[2]

Electrophysiology

AP-clamp sequential dissection experiments were conducted as described in our previous publication.[1] Cells were continuously superfused with a modified Tyrode solution (BTy) containing (in mmol/L) NaCl 120, KCl 5, $CaCl_2$ 2, $MgCl_2$ 1, 4-(2-Hydroxyethyl)piperazine-1-ethanesulfonic acid (HEPES) 10, $NaHCO_3$ 25, glucose 10, pH 7.3. The pipette solution contained (in mmol/L) K-Aspartate 115, KCl 45, Mg-ATP 3, HEPES 5, Adenosine 3′,5′-cyclophosphate (cAMP) 0.1, pH 7.25. Depending on the experiment, 0, 2, or 10 mM Ethylene glycol-bis(2-aminoethylether)-N,N,N′,N′-tetraacetic acid (EGTA) was added into the pipette solution. The basic experimental steps were as follows: (1) Record the steady-state AP under the I clamp (I = 0) at 1-Hz pacing frequency. (2) Apply this AP as the voltage command onto the same cell under the V clamp at 1 Hz. The net current output, I_{BG}, should be zero. (3) Isolate the current of interest by using its specific blocker to remove it from the net current output, I_{drug}. (4) The current of interest is then obtained by subtraction: $I = I_{BG} - I_{drug}$. (5) Next, isolate the 2nd current of interest by applying the 2nd channel blocker, and then obtain the 2nd current by subtraction: $I_2 = I_{drug1} - I_{drug2}$. Repeat step 5 to isolate the 3rd, the 4th, and more currents by sequentially adding the specific blocker for each channel (Table 1). The currents were recorded after they reached steady state. The inhibitory coefficient of SEA0400 on blocking I_{NCX} was measured by using a standard ramp V-clamp protocol.[3] The inhibitory coefficient of SEA0400 on blocking $I_{Ca,L}$ was measured by using a standard V-clamp protocol.[2]

All experiments were conducted at 21°C ± 1°C, except those in Figure 6, which were conducted at 36°C ± 0.5°C. Chemicals were purchased from Sigma-Aldrich, USA, except SEA0400, 2-[4-[(2,5-difluorophenyl)methoxy]phenoxy]-5-ethoxyaniline, which was provided by Taisho Pharmaceutical (Tokyo, Japan).

Table 1 Characteristic parameters of the currents measured at 21°C

Currents (pA/pF)	Ca^{2+} cycling (0 EGTA)	Ca^{2+} buffered (EGTA 10 mM)
I_{K1}	Ba^{2+} 50 μmol/L	
Diastolic	0.306 ± 0.305	0.281 ± 0.215
Peak	1.860 ± 0.386	1.723 ± 0.541
I_{Ks}	Chromanol-293B 10 μmol/L	
Diastolic	0.016 ± 0.064	−0.007 ± 0.138
Peak	0.340 ± 0.219	0.374 ± 0.208
I_{Kr}	E4031 1 μmol/L	
Diastolic	0.038 ± 0.031	0.004 ± 0.110
Peak	0.571 ± 0.161	0.724 ± 0.184*
I_{NIFE}	Nifedipine 10 μmol/L	
Diastolic	0.072 ± 0.151	0.103 ± 0.274
Peak	−1.434 ± 0.302	−2.36 ± 0.262†

Student's t test.
*$P < .05$, †$P < .001$ (n = 11–17 cells per group).

Results

Nifedipine-sensitive current during the AP with Ca^{2+} cycling

Ionic currents were recorded in ventricular cardiac myocytes by using the onion-peeling technique. First, we tested the effect of 0.1% Dimethyl sulfoxide; C_2H_6OS (DMSO), which is used as a solvent of drugs. Application of DMSO resulted in no change in the zero baseline current (Figure 1A). Nifedipine at 10 μM concentration was added into the bath to dissect out I_{NIFE}, as shown in Figure 1B. I_{NIFE} displays several distinct features. There is a steep rise in the current at phase 1 of the AP, which we named the initial current ("I") and measured it at 10 ms following the AP upstroke. During phase 2, the current slows down and forms a dome, which we named the dome current and measured it at APD10 (early plateau "E") and APD20 (dome "D") (APD# is defined as the AP duration measured at #% repolarization.) During phase 3, the current declines but then resurges to reach a second dome ("S"). Then, the current declines again and slowly diminishes during phase 4; we named this feature the residual current ("R") and measured it at 30 ms after $-V_{max}$ (the maximum repolarization rate of the AP during phase 3). While the initial phase and the dome features were seen before,[4,5] the second dome and the residual current during AP phases 3 and 4 are novel observations that had not been reported previously.

To confirm that I_{NIFE} originates from blocking the L-type Ca^{2+} channel, we used a different blocker, nisoldipine 1 μM, to record the nisoldipine-sensitive current (I_{NISO}) under the AP clamp. I_{NISO} (Figure 1C, n = 8 cells) displays the same distinct features and similar values as I_{NIFE} (Figure 1D, n = 8 cells).

Corresponding to the residual current, we also found a slowing down of the membrane repolarization at the end of the AP that extends beyond APD95 (Figure 1E), which we named *residual depolarization* and measured it as the voltage above the resting potential at 30 ms after $-V_{max}$ (the same time point for measuring the residual current). The residual depolarization had not been reported in the literature. However, we have consistently found this residual depolarization in both the single cell and the ventricular tissue (using sharp electrode recording of the AP, data not shown), confirming its existence in vivo. Furthermore, the

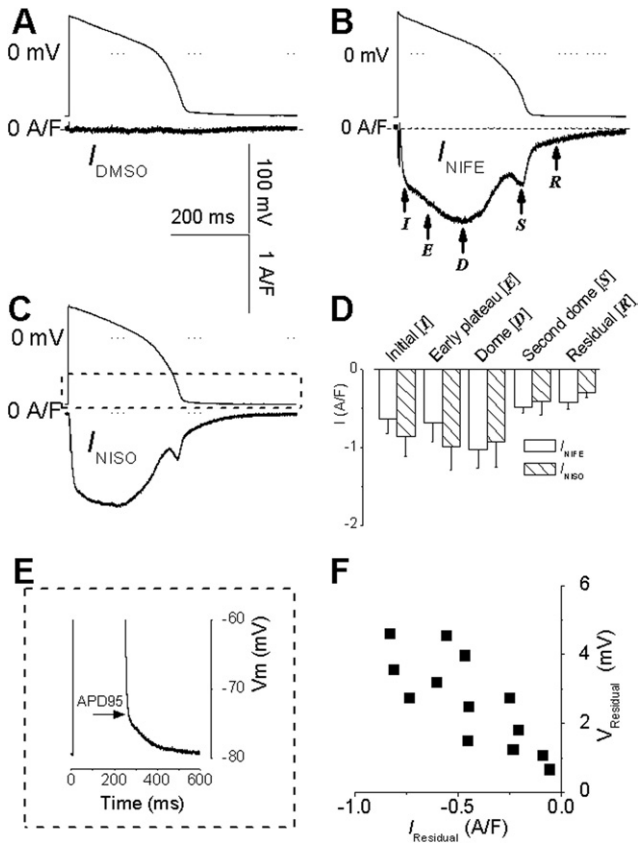

Figure 1 Panel A shows a representative current trace recorded with 0.1% (v/v) DMSO (used as a solvent of channel blockers). The flat "zero current" indicates a lack of any DMSO effect on membrane currents (n = 5 cells). Panels B and C are representative recordings of I_{NIFE} and I_{NISO}, respectively. Panel D shows the statistical comparison of I_{NIFE} (n = 7) and I_{NISO} (n = 5), demonstrating no significant differences between the currents. Panel E shows the residual depolarization. Panel F shows a positive correlation between the residual depolarization and the residual current measured at 30 ms after $-V_{max}$. I_{NIFE}, nifedipine-sensitive current; I_{NISO}, nisoldipine-sensitive current.

residual depolarization shows a strong positive correlation with the residual current (Figure 1F), indicating a connection between the 2.

I_{NIFE} consists of $I_{Ca,L}$ and I_{NCX}

I_{NIFE} is composed of not only $I_{Ca,L}$ but also I_{NCX} and other Ca^{2+}-sensitive currents. This is because blocking $I_{Ca,L}$ also eliminates the entry of Ca^{2+} into the cell to trigger sarcoplasmic reticullum (SR) Ca^{2+} release, which abolishes the intracellular Ca^{2+} transient and its associated currents such as the inward I_{NCX}, the Ca^{2+}-activated Cl^- current, and possibly a fraction of K^+ currents that is sensitive to Ca^{2+}. We conducted all experiments at 21°C to render the Cl^- current negligible.[6,7] To determine the Ca^{2+} sensitivity of K^+ currents, we used the onion-peeling method[1] to record I_{Ks} , I_{Kr} , I_{K1}, and I_{NIFE} in the same cell. The currents measured with Ca^{2+} cycling versus with EGTA are listed in Table 1. I_{K1} and I_{Ks} did not show any significant difference in the peak current density; peak I_{Kr} decreased slightly (0.15 A/F). However, the average peak current of I_{NIFE} was 1.4 A/F with Ca_{2+} cycling and 2.4 A/F with EGTA. Hence, the Ca^{2+}-sensitive component in K^+ currents is much smaller than the magnitude of I_{NIFE}, which should cause only a slight underestimation of I_{NIFE}. Therefore, the I_{NIFE} recorded in our experiment is mainly composed of $I_{Ca,L}$ and I_{NCX}.

Ca^{2+}-dependent features of I_{NIFE}

To separate the $I_{Ca,L}$ and I_{NCX} components in I_{NIFE}, we added 10 mM EGTA to the pipette solution to buffer intracellular Ca^{2+} and minimize the inward I_{NCX}. A typical recording of I_{NIFE} with 10 mM EGTA is shown in Figure 2A. Now the I_{NIFE} profile displays the *initial* current and the *dome* current features, but without any discernable *second dome* and *residual current*, different from that recorded with Ca^{2+} cycling (Figure 1B). Moreover, the residue depolarization is also eliminated (Figure 2B).

When EGTA concentration in the pipette was reduced from 10 to 2 mM, I_{NIFE} displayed the initial current and the dome current but the second dome was absent in all records. Buffering of Ca^{2+} eliminated the second dome and the residual current but elevated the dome current in a concentration-dependent manner (Figure 2A and 2C). These phenomena are visualized in the I–V relationship (Figure 2D) and confirmed in the statistical comparison of the current amplitudes along the AP time course (Figure 2E). Again, corresponding to a lack of the residual current the residual depolarization was also eliminated (Figure 2F). Note that low EGTA (2 mM) buffering can significantly affect Ca^{2+} and the dynamics of I_{NIFE} during AP.

Contribution of I_{NCX} to I_{NIFE}

The fact that buffering Ca^{2+} can eliminate the second dome and the residual current suggests that I_{NCX} might contribute to these features. To investigate this, we used an I_{NCX} inhibitor, SEA0400 at 3 μM concentration, to record the SEA-sensitive current (I_{SEA}). As shown in Figure 3A, I_{SEA} displays a small initial current at AP phase 1; gradually increases during phase 2, peaks at early phase 3 and declines; the current then turns around and reaches the second dome at late phase 3; and then declines to a residual current extending into phase 4. These data show that I_{NCX} dominates the late phases of AP. After I_{SEA} had developed and stabilized, we added 10 μM of nifedipine into the bath and recorded the $I_{SEA\ +\ NIFE}$ current (Figure 3B and 3C). Statistical comparison of the currents shows that the contribution of I_{NCX} to $I_{SEA\ +\ NIFE}$ is relatively small during the early phases of AP but becomes larger in later phases (Figure 3D).

Although SEA0400 is the most potent inhibitor of I_{NCX} currently available, it also partially blocks $I_{Ca,L}$. This means that I_{SEA} is composed of not only I_{NCX} but also a small portion of $I_{Ca,L}$. To separate I_{NCX} from $I_{Ca,L}$, we measured the inhibitory coefficients of 3 μM SEA0400 on I_{NCX} and $I_{Ca,L}$, respectively. The inhibitory effect of SEA0400 on I_{NCX} is voltage dependent, about 65% and 51% for the outward I_{NCX} measured at +30 mV and the inward I_{NCX} measured at −75 mV (Figure 3E and 3F). The inhibitory effect of 3 μM SEA0400 on $I_{Ca,L}$ is

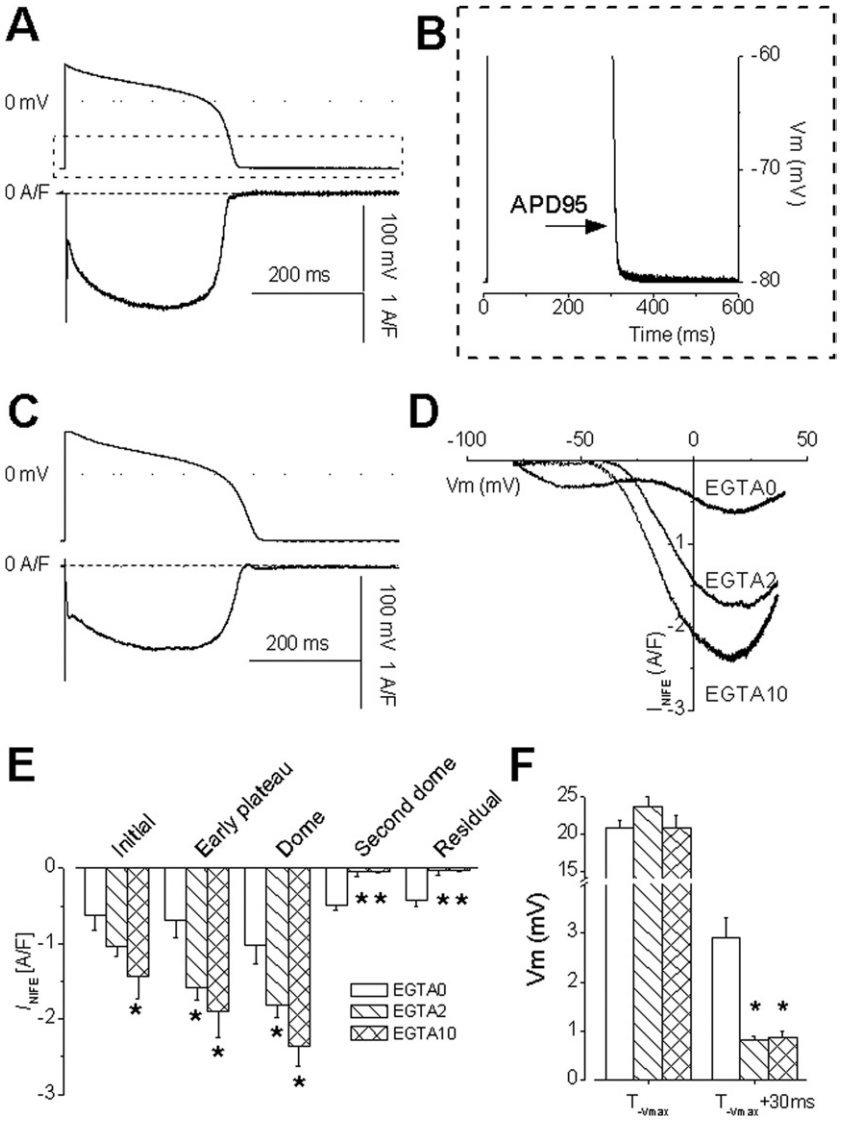

Figure 2 Representative I_{NIFE} recorded under the AP clamp with 10 mM EGTA in pipette (n = 10 cells). Notice an absence of the second dome, the residual current (**A**), and the residual depolarization (**B**). I_{NIFE} recorded with 2 mM EGTA (**C**, n = 14 cells), the current–voltage relationship (**D**), and statistical comparison between different Ca^{2+} buffering conditions (**E**) show increased current density with more EGTA buffering. Panel F demonstrates that EGTA did not affect the voltage at $-V_{max}$ but significantly reduced the residual depolarization at 30 ms after $-V_{max}$ (t test, $*P < .05$; $**P < .01$). AP, action potential; I_{NIFE}, nifedipine-sensitive current.

about 24% at the peak and is also voltage dependent (Figure 3G and 3H).

Reconstruction of $I_{Ca,L}$ and I_{NCX} during the AP

Both $I_{Ca,L}$ and I_{NCX} are heavily dependent on the local Ca^{2+} concentration. However, currently there is no available technique to *directly* measure the local Ca^{2+} concentrations sensed by the channel/transporter. To circumvent this problem, we took a simple approach to calculate $I_{Ca,L}$ and I_{NCX} from the paired recordings of I_{SEA} and $I_{SEA\ +\ NIFE}$ (using 2 equations to solve for 2 unknowns) by utilizing the differential inhibitory coefficients of SEA versus nifedipine. This simple calculation using paired recordings provides a somewhat direct approach to disentangle $I_{Ca,L}$ and I_{NCX}. Given that $I_{Ca,L}$ and I_{NCX} are the predominant currents blocked by nifedipine and SEA0400, the charge conservation gives the following equations:

$$I_{SEA+NIFE} = I_{Ca,L} + \alpha I_{NCX}$$

$$I_{SEA} = k_{Ca,L}(I_{Ca,L} + \alpha I_{NCX}) + k_{NCX}(1 - \alpha k_{Ca,L})I_{NCR}$$

where k_{CaL} and k_{NCX} are the voltage-dependent inhibitory coefficients of $I_{Ca,L}$ and I_{NCX} measured from the voltage-clamp experiments shown in Figure 3F and 3H. α is a scaling factor (ranging between 0 and 1 inclusive) that reflects the portion of I_{NCX} that is affected by changes in $I_{Ca,L}$. Because the local Ca^{2+} concentration sensed by the Na^+/Ca^{2+} exchanger is unknown, we solved the equations for $\alpha = 0$ and 1 to calculate the boundary conditions and estimate the currents. Figure 4 shows I_{NCX} and $I_{Ca,L}$ computed from paired recordings of I_{SEA} and $I_{SEA\ +\ NIFE}$ during the AP with Ca^{2+} cycling (column A) or with EGTA (column B). The current traces are shown in the upper row. Notice that I_{SEA} is an inward current due to the forward-mode I_{NCX} when Ca^{2+} is cycling but turns into an outward current due to the reverse-mode I_{NCX} when Ca^{2+} is buffered with 10 mM EGTA. The $I_{Ca,L}$ and I_{NCX} calculated from I_{SEA} and $I_{SEA\ +\ NIFE}$ are shown in Figure 4 (middle and lower row). The blue ($\alpha = 1$) and red ($\alpha = 0$) traces demarcate the upper and the lower boundaries of the currents, respectively. The actual current should fall within the

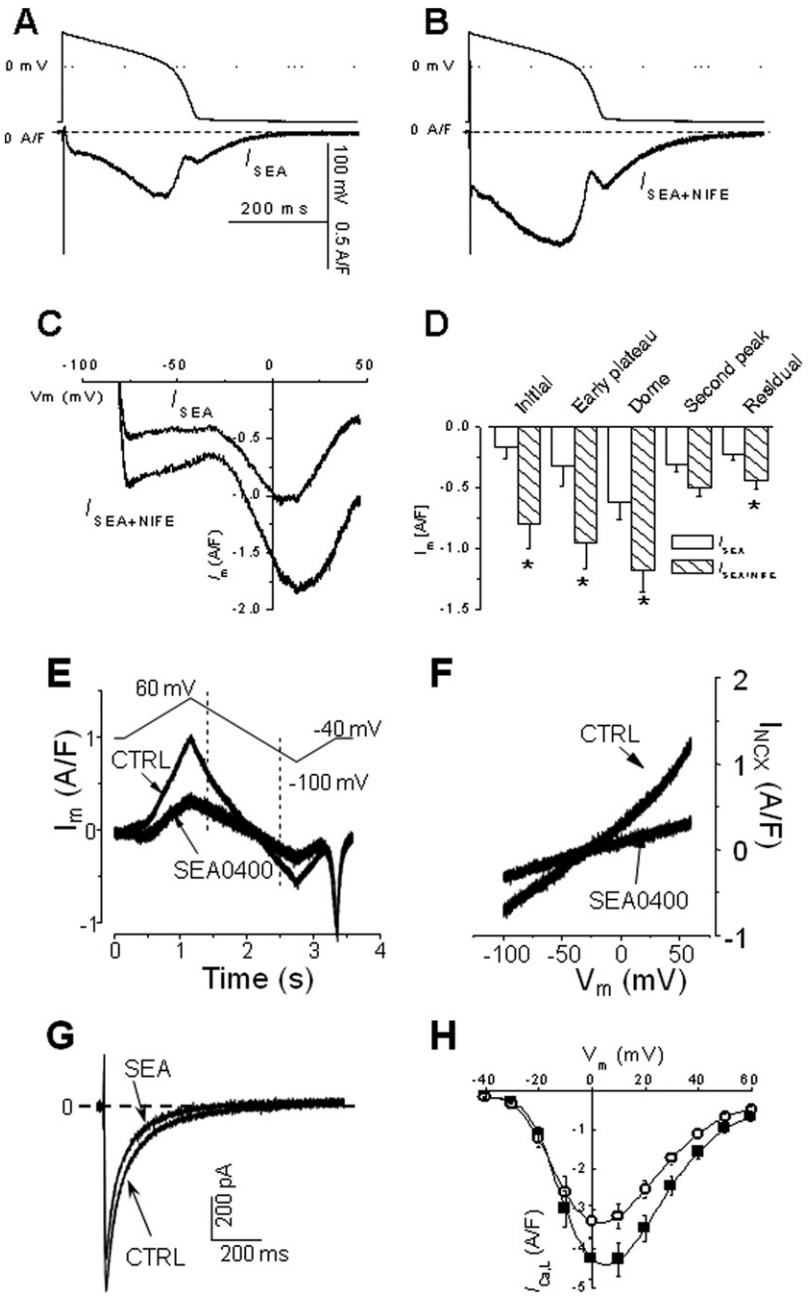

Figure 3 Panel A shows a representative current recorded with 3 μM SEA0400 (I_{SEA}). When 10 μM nifedipine was added, $I_{SEA\ +\ NIFE}$ displays similar characteristics (**B**). Panels C and D show the instant current–voltage relationship of I_{SEA} and $I_{SEA\ +\ NIFE}$ and statistical comparison of data (n = 7 cells, t test, $*P < .05$). Standard V-clamp protocols were used to measure the inhibitory effects of 3 μM SEA. Panels E and F show current traces and the I–V relationship of I_{NCX} before and after the application of SEA. Panels G and H show representative current traces and the I–V relationship of $I_{Ca,L}$ before and after the application of SEA. $I_{Ca,L}$, L-type Ca^{2+} current; I_{SEA}, SEA-sensitive current.

boundaries. Note that I_{NCX} is bounded within a narrow range; hence, the profile of I_{NCX} during the AP is clearly defined. A probable profile of the current is highlighted with a black line (calculated as an intermediate state with α = 0.8).

The magnitude of $I_{Ca,L}$ dome current is about 0.3 A/F when Ca^{2+} is normally cycling (column A, middle panel) but becomes much greater to about 2 A/F when Ca^{2+} is buffered (column B, middle panel). This difference reflects a profound influence of the Ca^{2+}-dependent inactivation (CDI) of $I_{Ca,L}$. Note also that buffering Ca^{2+} completely eliminated the second dome and the residual current. When Ca^{2+} is cycling, I_{NCX} is briefly outward at the beginning of AP but soon becomes an inward current (column A, lower panel) and reaches a peak of about 0.2 A/F. In contrast, when Ca^{2+} is buffered, I_{NCX} is always outward during the AP (column B, lower panel).

Effects of SEA0400

It has been proposed that inhibiting I_{NCX} might provide an effective therapy for some forms of arrhythmias. We predicted that using SEA0400 to treat the cell would reduce the dome current and the residual current. To test this, we pretreated cells with 3 μM SEA0400 and recorded the remaining I_{NIFE} under the AP clamp. As shown in Figure 5A, SEA0400 treatment shortened APD, consistent with its effect on reducing the dome and the residual current.

A representative trace of the I_{NIFE} in the SEA0400-pretreated cell is shown in Figure 5B. Recall that in the control cell (Figure 1B) the dome is larger than the initial

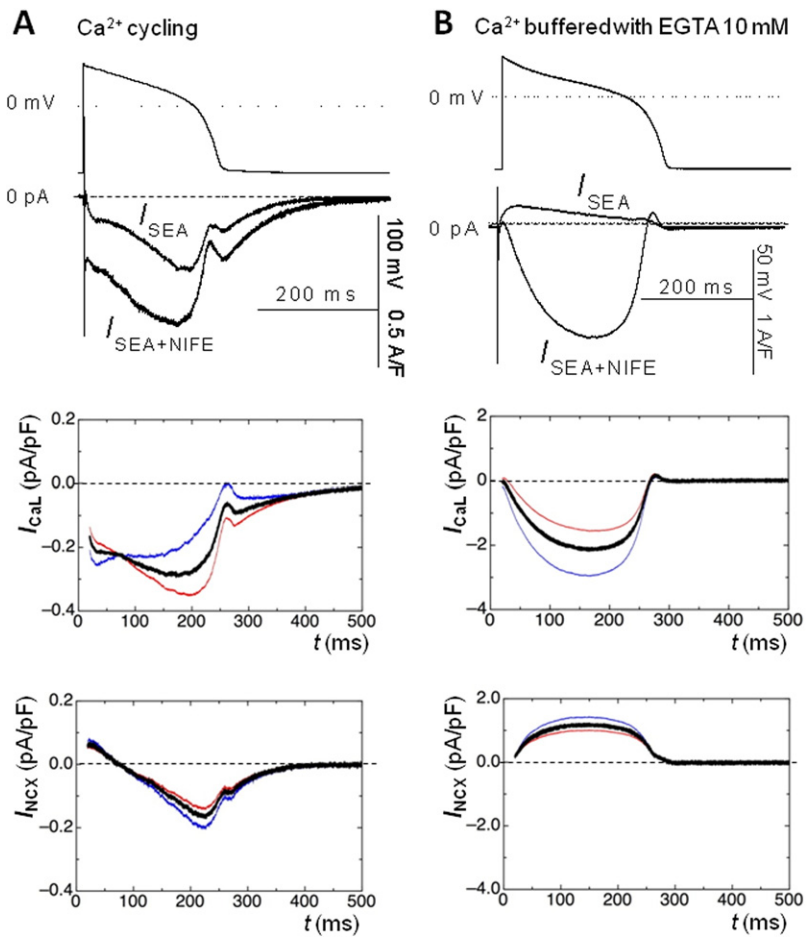

Figure 4 Columns A and B show I_{SEA} and $I_{SEA\ +\ NIFE}$ recorded in the absence and presence of EGTA, respectively. EGTA buffering of Ca^{2+} reversed I_{SEA} and amplified $I_{SEA\ +\ NIFE}$. Mathematical reconstruction of $I_{Ca,L}$ and I_{NCX} assuming zero coupling ($\alpha = 0$, red line) or linear coupling ($\alpha = 1$, blue line) between $I_{Ca,L}$ and I_{NCX} mark the boundaries of the actual currents. The black line shows an intermediate state ($\alpha = 0.8$), highlighting a probable profile of the currents. $I_{Ca,L}$, L-type Ca^{2+} current; I_{NCX}, Na^+/Ca^{2+} exchange current; I_{SEA}, SEA-sensitive current.

current; here, in the SEA0400-pretreated cell the dome becomes smaller than the initial current, indicating that a portion of the dome current is contributed by the inward I_{NCX}. The residual current is significantly smaller after SEA0400 treatment (Figure 5C), consistent with the I_{NCX} contribution. Meanwhile the residual depolarization is also smaller (Figure 5D). In fact, a positive correlation between the residual current and the residual depolarization exists universally for all the experimental conditions tested (Figure 5E), indicating that the residual current is responsible for the residual depolarization.

I_{NIFE} at body temperature

To establish the physiological relevance of our new findings, we also conducted AP-clamp experiments at body temperature. The I_{NIFE} at 36°C displays essentially the same features (Figure 6A). The second dome and the residual currents are prominent, and the residual depolarization is also present (Figure 6B). The insert shows the Ca^{2+} transient measured with Fura-2. Using EGTA to buffer Ca^{2+} eliminates the residual current (Figure 6C) and the residual depolarization (Figure 6D). Statistical comparison shows that with Ca^{2+} cycling, the dome current is significantly smaller (Figure 6E) due to the CDI of $I_{Ca,L}$, but the residual current and the residual depolarization are significantly larger (Figure 6E and 6F) due to the inward I_{NCX}.

Discussion

Here we present experimental measurements of $I_{Ca,L}$ and I_{NCX} currents during the AP with Ca^{2+} cycling in ventricular myocytes. This was enabled by a triad of conditions: (1) using the cell's own AP as the voltage command; (2) using the internal and external solutions that mimic the physiological milieu; and (3) preserving Ca^{2+} cycling during the AP by not using exogenous Ca^{2+} buffer. To the best of our knowledge, it is the first time that this triad of conditions has been used to record the ionic currents during cardiac AP with Ca^{2+}cycling.

I_{NIFE} was obtained by blocking L-type Ca^{2+} current under the AP clamp. However, blocking Ca^{2+} current also affects other Ca^{2+}-dependent currents including I_{NCX}, Ca^{2+}-activated Cl^- current, and the Ca^{2+}-sensitive components in K^+ currents. The Cl^- current was rendered negligible by conducting experiments at 21°C.[6,7] We also found no significant contributions of K^+ currents. Hence, I_{NIFE} mainly consists of $I_{Ca,L}$ and I_{NCX}. The profile of I_{NIFE} during the AP exhibits distinct features: an *initial* current at phase 1, a *dome* at phase 2, a resurging *second dome* at phase 3, and a *residual* current at phase 4. The second dome and the residual current had not been reported before; these novel features become apparent only when Ca^{2+} is not buffered. We also detected a hitherto unreported residual

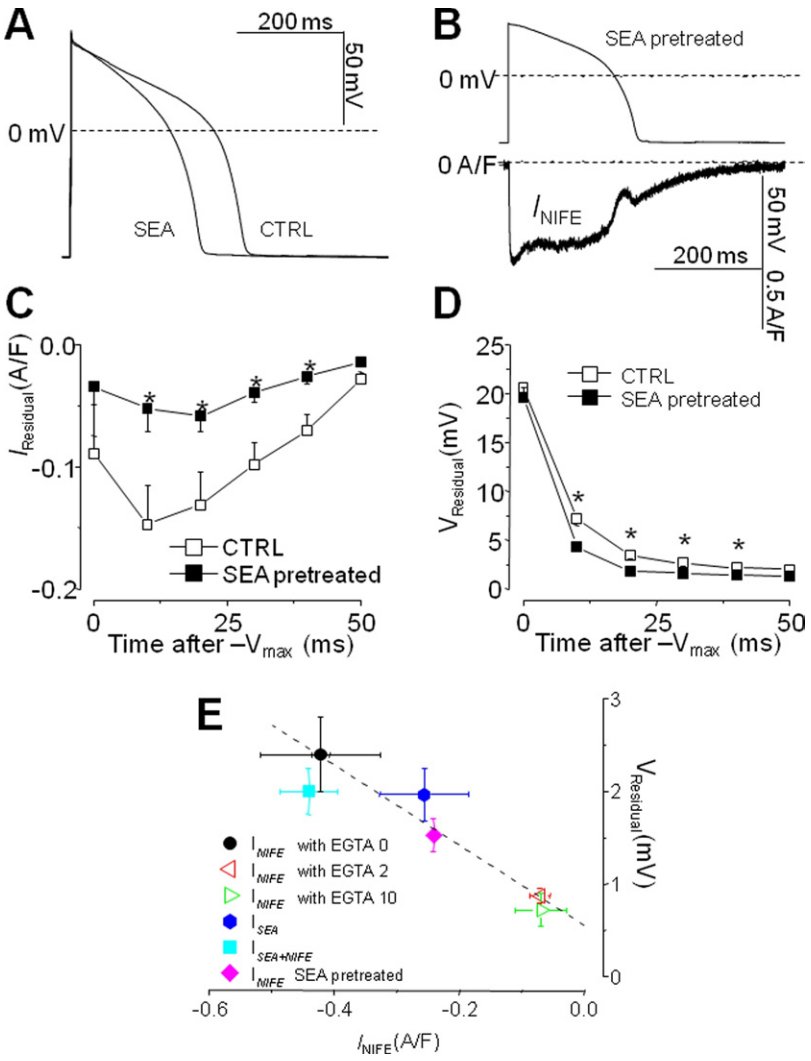

Figure 5 Using 3 μM SEA0400 to treat cells shortened the AP duration (**A**) and reduced I_{NIFE} (**B**). The residual current (**C**) and the residual depolarization (**D**) were significantly reduced (n = 7 cells, t test, $^*P < .05$), demonstrating a predominant influence of I_{NCX} on these features. Panel E shows a universal correlation (r = 0.917) between the magnitude of residual current and residual depolarization under all experimental conditions tested. AP, action potential; I_{NCX}, Na^+/Ca^{2+} exchange current; I_{NIFE}, nifedipine-sensitive current.

depolarization at the end of the AP that can be attributed to the residual current. Furthermore, we found that $I_{Ca,L}$ contributes predominantly to the initial and the dome current whereas I_{NCX} contributes significantly to the second dome and the residual current. The timing and magnitude of these currents suggest their relative roles in shaping the AP profile and generating early or delayed afterdepolarizations.

The dynamic profile of $I_{Ca,L}$ during cardiac AP and its contribution to afterdepolarizations has been under active investigation. Previous studies used variants of the AP-clamp technique and reported the initial current and the dome current features but never before reported the second dome and the residual current features. This discrepancy can be explained by the experimental conditions used in those studies, which differed from the triad of conditions used in our experiments. First, in earlier studies the AP waveform used as voltage command was either a representative AP[5] or a constructed AP,[8] which does not, in general, match each cell's unique AP. Hence, the current profile would be distorted from its natural state in the cell. Second, earlier experiments used nonphysiological solutions (substituting Na^+ and K^+), but ion species and concentration are known to alter the Ca^{2+} channel kinetics.[9,10] Third, most earlier experiments used exogenous Ca^{2+} buffer, and the $I_{Ca,L}$ profile reported in those studies is similar to the I_{NIFE} profile recorded with EGTA in our study (Figure 2A and 2C). The second dome and the residual current in I_{NIFE} are novel features revealed only under the triad of conditions used in our AP-clamp experiments.

The dynamic profile of $I_{Ca,L}$ during the AP is determined by an interplay between the changing driving force during the AP and CDI. Importantly, our data show a significant modulation of $I_{Ca,L}$ during the AP by CDI, seen as the I_{NIFE} dome current increases with EGTA in a dose-dependent manner (Figure 2E). The average dome current is 1.4 pA/pF when Ca^{2+} is cycling, and this increases to 2.4 pA/pF when Ca^{2+} is buffered with 10 mM EGTA. It is noteworthy that previous voltage-clamp and AP-clamp studies (using Ca^{2+} buffer) reported a peak $I_{Ca,L}$ between 2 and 10 pA/pF; quantitative models based on those data also had a peak $I_{Ca,L}$ in that range.[11] Our data show a much smaller $I_{Ca,L}$ magnitude in the cell measured under the AP clamp with Ca^{2+} cycling and provide realistic experimental data for future modeling considerations.

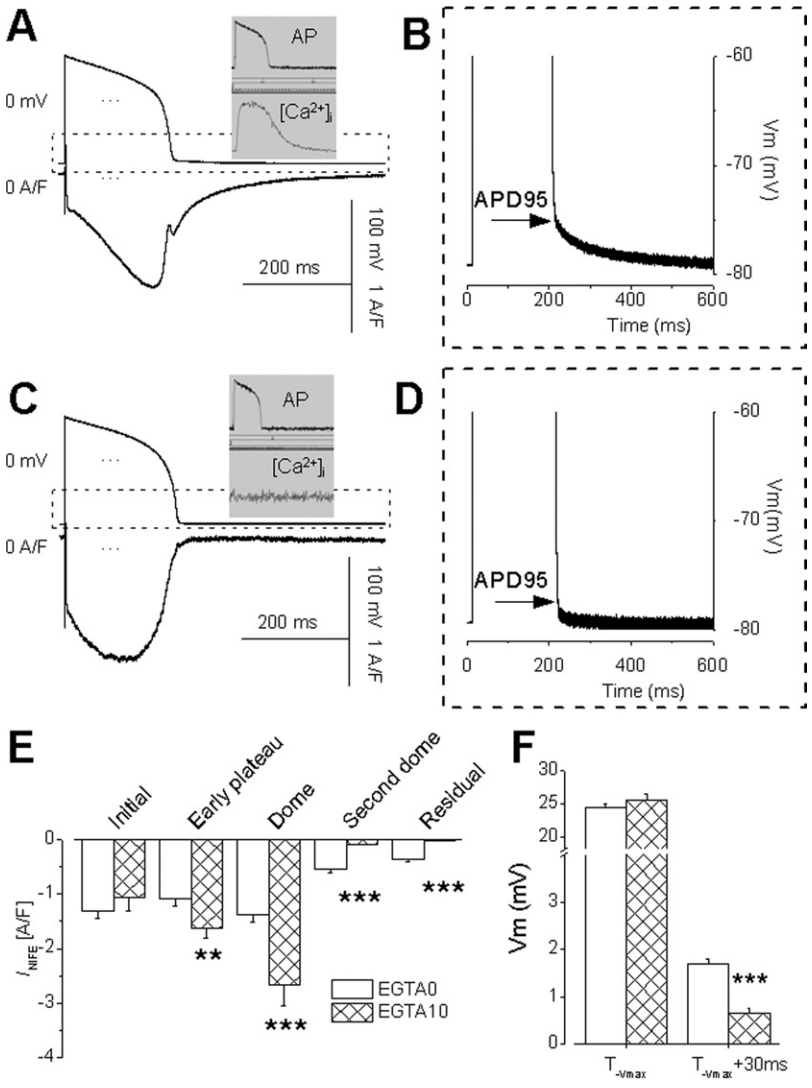

Figure 6 These experiments were conducted at 36°C. Panel A shows a representative I_{NIFE} recorded under the AP clamp with Ca^{2+} cycling (n = 19 cells). Notice the presence of the second dome and the residual current (**A**) and the residual depolarization (**B**). The insert shows the Ca^{2+} transient measured with Fura-2. Panel C shows a representative I_{NIFE} recorded with 10 mM EGTA (n = 9 cells). Notice the absence of the residual current (**C**) and the residual depolarization (**D**). Panels E and F show the mean ± SE and statistical comparison at the features points (t test, $^{**}P < .01$, $^{***}P < .001$). AP, action potential; I_{NIFE}, nifedipine-sensitive current.

Previously, a lack of a selective blocker prevented direct measurement of I_{NCX}.[12] In this study, we used SEA0400 paired with nifedipine to isolate the I_{NCX} during the AP with Ca^{2+} cycling. Our data reveal that I_{NCX} presents an outward current at the beginning of the AP, which turns into a small inward current at early phase 2; the inward I_{NCX} increases and contributes significantly to the I_{NIFE} second dome and the residual current at phases 3 and 4. In comparison to earlier studies, Grantham and Cannell[5] had calculated an I_{NCX} profile that showed a large outward current throughout AP phases 1 and 2, then turned into an inward current at phase 3, and then peaked at the end of phase 3. Weber et al[13] reconstructed the I_{NCX} during the AP by correlating the Ca^{2+} transient with the steady-state I_{NCX} measurements at various Ca^{2+} concentrations. They showed in rabbit ventricular myocytes that I_{NCX} was a rapid outward current at phase 1, turned to inward at early phase 2, reached a peak at the end of phase 3, and then slowly declined during phase 4. The I_{NCX} profile in Figure 4 (column A, lower panel) shows similar features as their result but differs in the time course and the magnitude of current. Given the importance of I_{NCX} in shaping the AP, our AP-clamp measurement of I_{NCX} in the physiological milieu provides important data for developing more accurate quantitative models.

Increased $I_{Ca,L}$ or I_{NCX} had been found to induce afterdepolarizations.[14,15] Inhibiting $I_{Ca,L}$ with Ca^{2+} channel-blocker effectively eliminated early afterdepolarizations.[14,16,17] Inhibiting I_{NCX} with SEA0400 also effectively reduced early and delayed afterdepolarizations.[3,12] Hence, $I_{Ca,L}$ and I_{NCX} have been proposed as therapeutic targets for treating cardiac arrhythmias (see review by Sipido et al[12]). The relative contributions of $I_{Ca,L}$ and I_{NCX} to the depolarization drive are resolved in the current study. As we observed, $I_{Ca,L}$ is the dominant inward current during AP phases 1 and 2, whereas I_{NCX} is the dominant inward current during phases 3 and 4. Both $I_{Ca,L}$ and I_{NCX} contribute to the dome current, the second dome, and the residual current. Given the intertwined nature of $I_{Ca,L}$ and I_{NCX}, it is the combination of these 2 currents, not just one or the other, that determines the total depolarization drive that shapes the AP profile and afterdepolarizations.[18] Importantly, the newly observed second dome and the residual

current occurring at phases 3 and 4 have the right timing and the shape to generate afterdepolarizations if not counterbalanced by repolarizing currents. Our data clearly show that the second dome coincides with the vulnerable phase of the AP where early afterdepolarizations may develop, while delayed afterdepolarizations may occur where we observed the residual current. The current study provides useful and physiologically relevant data to aid quantitative modeling of cardiac AP and rational design of antiarrhythmia drug therapies.

Acknowledgments

We thank Shaden Khabbaz, Charles Payne, and Stephanie E. Edelmann for their excellent work in isolating cardiac cells. We are grateful to Dr Robert Hadley (University of Kentucky) for kindly providing cells for our early experiments. We are also grateful to Dr Donald M. Bers and Dr Kenneth Ginsburg and Taisho Pharmaceutical (Tokyo, Japan) for the generous gift of SEA0400. Our gratitude also goes to Dr Donald M. Bers (University of California) and Dr Mark E. Anderson (University of Iowa) for reading early drafts of the manuscript and contributing insightful comments.

References

1. Banyasz T, Horvath B, Jian Z, Izu LT, Chen-Izu Y. Sequential dissection of multiple ionic currents in single cardiac myocytes under action potential-clamp. J Mol Cell Cardiol 2011;50:578–581.
2. Chen-Izu Y, Chen L, Banyasz T, et al. Hypertension-induced remodeling of cardiac excitation-contraction coupling in ventricular myocytes occurs prior to hypertrophy development. Am J Physiol Heart Circ Physiol 2007;293:H3301–H3310.
3. Birinyi P, Acsai K, Banyasz T, et al. Effects of SEA0400 and KB-R7943 on Na^+/Ca^{2+} exchange current and L-type Ca^{2+} current in canine ventricular cardiomyocytes. Naunyn Schmiedebergs Arch Pharmacol 2005;372:63–70.
4. Linz KW, Meyer R. Profile and kinetics of L-type calcium current during the cardiac ventricular action potential compared in guinea-pigs, rats and rabbits. Pflügers Archiv Eur J Physiol 2000;439:588–599.
5. Grantham CJ, Cannell MB. Ca^{2+} influx during the cardiac action potential in guinea pig ventricular myocytes. Circ Res 1996;79:194–200.
6. Nakajima I, Watanabe H, Iino K, Saito T, Miura M. Ca^{2+} overload evokes a transient outward current in guinea-pig ventricular myocytes. Circ J 2002;66:87–92.
7. Puglisi JL, Yuan W, Bassani JWM, Bers DM. Ca^{2+} influx through Ca^{2+} channels in rabbit ventricular myocytes during action potential clamp: influence of temperature. Circ Res 1999;85:e7–e16.
8. Linz KW, Meyer R. Control of L-type calcium current during the action potential of guinea-pig ventricular myocytes. J Physiol 1998;513:425–442.
9. Linz KW, Meyer R. Modulation of L-type calcium current by internal potassium in guinea pig ventricular myocytes. Cardiovasc Res 1997;33:110–122.
10. Hess P, Lansman JB, Tsien RW. Calcium channel selectivity for divalent and monovalent cations: voltage and concentration dependence of single channel current in ventricular heart cells. J Gen Physiol 1986;88:293–319.
11. Faber GM, Silva J, Livshitz L, Rudy Y. Kinetic properties of the cardiac L-type Ca^{2+} channel and its role in myocyte electrophysiology: a theoretical investigation. Biophys J 2007;92:1522–1543.
12. Sipido KR, Bito V, Antoons G, Volders PG, Vos MA. Na/Ca exchange and cardiac ventricular arrhythmias. Ann N Y Acad Sci 2007;1099:339–348.
13. Weber CR, Piacentino V, Ginsburg KS, Houser SR, Bers DM. Na-Ca exchange current and submembrane $[Ca^{2+}]$ during the cardiac action potential. Circ Res 2002;90:182–189.
14. January CT, Riddle JM. Early afterdepolarizations: mechanism of induction and block. A role for L-type Ca^{2+} current. Circ Res 1989;64:977–990.
15. Pogwizd SM, Qi M, Yuan W, Samarel AM, Bers DM. Upregulation of Na^+/Ca^{2+} exchanger expression and function in an arrhythmogenic rabbit model of heart failure. Circ Res 1999;85:1009–1019.
16. Anderson ME, Braun AP, Wu Y, et al. KN-93, an inhibitor of multifunctional Ca/calmodulin-dependent protein kinase, decreases early afterdepolarizations in rabbit heart. J Pharmacol Exp Ther 1998;287:996–1006.
17. Yamada MOK, Niwa A, Tsujino N, Nakada T, Hirose M. Contribution of L-type Ca^{2+} channels to early afterdepolarizations induced by I Kr and I Ks channel suppression in guinea pig ventricular myocytes. J Membr Biol 2008;222:151–166.
18. Weiss JN, Garfinkel A, Karagueuzian HS, Chen P-S, Qu Z. Early afterdepolarizations and cardiac arrhythmias. Heart Rhythm 2010;7:1891–1899.